Proposition of a simplified geomechanical model for compaction in sedimentary basins

Francesco Saverio Patacchini, Marie-Christine Cacas-Stentz, Nicolas Maurand, Walid Saber-Cherif, Françoise Willien

Proposition of a simplified geomechanical model for compaction in sedimentary basins

Francesco Saverio Patacchini[a,1,*], Marie-Christine Cacas-Stentz[a,2], Nicolas Maurand[a,b,3], Walid Saber-Cherif[4], and Françoise Willien[a,5]

[a] *IFP Energies nouvelles, 1 et 4 avenue de Bois-Préau, 92852 Rueil-Malmaison, France*
[b] *CEA, Cadarache F-13108 Saint-Paul-Lez-Durance, France*

[1] *francesco.patacchini@ifpen.fr* [2] *marie-christine.cacas-stentz@ifpen.fr*
[3] *nicolas.maurand@ifpen.fr* [4] *walid.sc@gmail.com* [5] *francoise.willien@ifpen.fr*
[*] *Corresponding author*

March 30, 2022

Abstract

In geomechanical modeling, it is a central task to predict the distribution of rock porosity throughout the burial history of a given sedimentary basin. In the upper layers, the evolution of porosity is mainly driven by the mechanical compaction resulting from sediment deposition on the top and from horizontal tectonic loading, so that compaction is indeed three-dimensional. Nevertheless, for simplicity, it is classical in basin simulators to assume oedometric conditions, that is, to neglect the lateral deformations, and thus to describe compaction as a one-dimensional phenomenon by relying on a vertical porosity-stress law. In this paper, we introduce a simple model which includes lateral deformations and whose goal is to improve the results obtained with oedometric modeling without losing much computational time. The model is based on a modified vertical porosity-stress law in which horizontal strains are inserted and on an elastic stress-strain law with stress-dependent Young modulus. This gives rise to a *simplified* geomechanical model, as opposed to a full-dimensional, elastoplastic model. Still, we manage to validate the model on a geometrically and lithologically complex test case by comparing our results with those obtained on the same case using a three-dimensional finite-element simulator. We conclude that our model offers a significant improvement in accuracy compared to an oedometric model, especially in the undrained, deeper layers of the basin, without much loss in computational time. In this respect, the model provides a useful tool to users who might need a first, quick insight into results before engaging in longer and more accurate simulations.

Keywords: sedimentary basin, mechanical compaction, horizontal deformation, geomechanical model, finite-volume simulator

1 Introduction

When modeling the evolution of a sedimentary basin, one is often interested in determining the changes in rock porosity and permeability taking place over

a geological time interval. Indeed, these quantities control the overpressure distribution in the basin and need to be predicted, for instance, for drilling risk assessment [36]. Since permeability is obtained directly from porosity via the Kozeny–Carman law [11, 12, 27] or other sediment-specific laws [17, 43], we choose porosity as our main unknown.

Porosity evolution is mainly driven by mechanical and chemical compaction [25]. Usually, mechanical compaction is the dominating phenomenon in the upper layers of the basin, while chemical compaction dominates in the lower layers. The depth transition between mechanically and chemically dominated layers depends on lithology, varying from 0.1 km for carbonates [2, 18] to 1.5 km for sandstone [6, 20, 22, 34]. In the present work, we neglect chemical compaction so that our model is best suited, but not limited, to upper layers.

Because mechanical compaction is mostly driven by gravity through burial, it is often described as a vertical, thus one-dimensional, phenomenon in basin models [13, 23, 31, 33] and simulators [15, 40, 42]. This approach provides good accuracy in oedometric contexts, where the horizontal strains are negligible. However, since possibly horizontal phenomena having a significant influence on porosity occur [28, 32], e.g., as a result of tectonics, this is not entirely satisfactory.

One solution is proposed in [25], where Schneider's porosity-stress law [35, 38] is integrated into the Drucker–Prager model for plasticity [14], resulting in a three-dimensional compaction model. This model is tested numerically in [3, 9, 25] using the prototype code A^2, which sequentially couples the finite-volume basin simulator ArcTem [20] with the finite-element geomechanical simulator Code Aster [19] following an iterative algorithm [26]. (See [8] for further A^2 simulations in the context of rock failure.) This approach reaches very good accuracy but requires long simulation times due to its three-dimensional formulation.

Here, rather than derive a three-dimensional model such as in [25], we simply insert the horizontal strains into the vertical porosity-stress law and so keep a one-dimensional compaction model without neglecting the remaining dimensions. More precisely, we define an approximated porosity using a vertical porosity-stress law where the horizontal strains are added to the vertical stress; we then suppose that the approximated porosity is close to the actual one. For this closeness supposition to be justified, we need to insert the horizontal strains in a physically motivated way. In this paper, we propose one formulation based on an elastic stress-strain constitutive law with stress-dependent Young modulus. We thus suppose that the basin is an elastic medium, as opposed to elastoplastic, and consequently place ourselves in the context of small deformations. We refer to this method as *simplified geomechanical model*, where "simplified" contrasts with the more complex three-dimensional, elastoplastic approach of [25]. This simplified model bears a similarity with that investigated in [29], namely, that the vertical porosity-stress law is altered to account for a specific effect: in our case, the three-dimensional mechanical strain; in their case, the anisotropy.

Our main goal is to improve the results obtained with the oedometric assumption, in particular in the more strained lower layers, without losing significant computational time. Of course, as already mentioned, this entails simplifying assumptions, such as purely elastic deformations and a one-dimensional porosity-

stress law, so that our approach is by no means intended to reach the accuracy of any full-dimensional, elastoplastic model such as presented in [25]. Furthermore, we neglect the effects of the lateral deformations on the temperature; see for example [10] for a complete thermal model. Rather, we expect our model to be useful to users who might need a first, quick idea of the basin's porosity distribution before deciding whether to pursue more accurate and longer simulations. Our model is integrated entirely in ArcTem.

In Section 2, we recall the standard equations underlying the fluid and solid mechanics of a sedimentary basin; we place ourselves in the setting of a single-phase water flow. This section can be skipped by the experienced geomechanist and can be referred to only for notation. We then discuss in details mechanical compaction (simply referred to as compaction in the sequel) and present our simplified geomechanical model in Section 3. Then, Section 4 is dedicated to the numerical results obtained with our model coded in ArcTem and applied to a large test case modeling the Vaca Muerta formation of the Neuquén basin in Argentina. This test case covers a surface of about $35\,000\,\mathrm{km}^2$ and spans a time interval of 10 My. Our results under both oedometric and non-oedometric conditions are compared with those obtained using A^2 in [3] with the model derived in [25]. Furthermore, CPU times are given for various strain configurations. Finally, we summarize our results and give an outlook in Section 5.

2 Standard porous medium model

We briefly discuss the standard equations that we use to model the flow and mechanical equilibrium in our porous medium, i.e., our sedimentary basin. We also give the corresponding boundary and initial conditions.

2.1 Model equations

We write ϕ the Eulerian porosity of the medium and $\boldsymbol{V}_\alpha$ the velocity field associated with phase $\alpha \in \{s, w\}$ (solid or water). We write ρ_α the density of phase α and $\bar{\rho}_s = \rho_s(1-\phi)$ and $\bar{\rho}_w = \rho_w\phi$ the effective densities. The medium is assumed to be fully saturated with water.

By convention, we orient the orthonormal basis $(\boldsymbol{x}, \boldsymbol{y}, \boldsymbol{z})$ anticlockwise so that $\boldsymbol{z}$ points upwards and gravity reads $\boldsymbol{g} = (0, 0, -g)$ with $g > 0$. The origin of the corresponding axis triplet (x, y, z) is situated at the present sea level so that $z = 0$ at the sea surface and the basin can have either negative or positive z-coordinates.

2.1.1 Flow

We give here the equations on water and solid flow.

Conservation of mass. For any phase $\alpha \in \{s, w\}$ we have conservation of mass:

$$\frac{\partial \bar{\rho}_\alpha}{\partial t} + \operatorname{div}(\bar{\rho}_\alpha \boldsymbol{V}_\alpha) = q_\alpha, \tag{2.1}$$

where q_α is the rate of deposit of phase α due to sedimentation at the top of the basin and $\boldsymbol{V}_\alpha$ is the velocity of phase α.

Darcy's law. The filtration, or mean percolation, velocity $\boldsymbol{U}_w := \phi(\boldsymbol{V}_w - \boldsymbol{V}_s)$ is assumed to be small enough to follow Darcy's law, that is,

$$\boldsymbol{U}_w = \eta_w \boldsymbol{K}(-\boldsymbol{\nabla} p_w + \bar{\rho}_w \boldsymbol{g}), \tag{2.2}$$

where η_w is the water mobility, $\boldsymbol{K}$ the permeability tensor and p_w the water, or pore, pressure.

Densities. The solid density is assumed to be constant and the water density to follow a law which is linear in pressure p_w and temperature T:

$$\rho_s = \rho_{s,0} \quad \text{and} \quad \rho_w = \rho_{w,0}(1 + \alpha_w(T - T_0) + \beta_w(p_w - p_0)), \tag{2.3}$$

where T_0 and p_0 are reference values for the temperature and water pressure, $\rho_{s,0}$ and $\rho_{w,0}$ are reference densities, α_w is the water thermal expansion and β_w is the water compressibility. These laws are justified as long as the solid phase is incompressible and thermally unexpansible and the water phase is weakly compressible and weakly thermally expansible.

Water mobility. The water mobility is assumed to be temperature-dependent. Specifically,

$$\eta_w = a_w \left(T + \sqrt{b_w + T^2} - c_w \right), \tag{2.4}$$

where a_w, b_w and c_w are fitting parameters. If the basin is supposed to be isothermal, then the water mobility in (2.4) is constant and the water density in (2.3) only depends on temperature.

Permeability. The permeability tensor $\boldsymbol{K}$ is given by

$$\boldsymbol{K} = K(\phi)\boldsymbol{A}, \tag{2.5}$$

where $\boldsymbol{A}$ is an anisotropy tensor and K follows the Kozeny–Carman law [11,12,27]:

$$K(\phi) = \begin{cases} \dfrac{k_1 \phi^{n_1}}{S_0^2 (1-\phi)^{m_1}} & \text{if } \phi \leqslant \phi_0, \\ \dfrac{k_2 \phi^{n_2}}{S_0^2 (1-\phi)^{m_2}} & \text{if } \phi > \phi_0, \end{cases}$$

where S_0 is the specific surface area of the porous medium and k_1, k_2, n_1, n_2, m_1, m_2 and ϕ_0 are constants related to lithology. To ensure the continuity of K at ϕ_0, we impose the following relation on the parameters:

$$\frac{\phi_0^{n_2 - n_1}}{(1-\phi_0)^{m_2 - m_1}} = \frac{k_1}{k_2}.$$

2.1.2 Temperature and mechanical equilibrium

We now discuss the equations for temperature distribution and mechanical equilibrium in the basin.

Temperature. We suppose that the temperature of the basin obeys a very simple vertical model, namely,

$$\frac{\partial T}{\partial z} = G, \tag{2.6}$$

where G is a known temperature gradient, sometimes referred to as geothermal gradient, which may depend on position and time. We refer the reader to [10] for an example of geomechanical model including the effects of large strains on the temperature, which we do not consider here.

Mechanical equilibrium. We denote by $\boldsymbol{\sigma}$ the Cauchy stress tensor. This tensor includes both water and solid stresses and is therefore sometimes referred to as *total* stress tensor. We write

$$\boldsymbol{\sigma} = \begin{pmatrix} \sigma_x & \sigma_{xy} & \sigma_{xz} \\ \sigma_{xy} & \sigma_y & \sigma_{yz} \\ \sigma_{xz} & \sigma_{yz} & \sigma_z \end{pmatrix}, \tag{2.7}$$

where σ_i and σ_{ij} are the normal and shear stresses for all $i, j \in \{x, y, z\}$ with $j \neq i$. We use the sign convention according to which a normal stress is positive when there is compression in its direction.

By Cauchy's momentum equation, mechanical equilibrium is given by

$$\operatorname{div} \boldsymbol{\sigma} = \bar{\rho}\boldsymbol{g} + \boldsymbol{f}, \tag{2.8}$$

where $\bar{\rho} := \bar{\rho}_w + \bar{\rho}_s$ is the homogenized density and $\boldsymbol{f} := (f_x, f_y, f_z)$ is the vector containing the volumic external forces other than gravity. More explicitly, (2.8) rewrites as

$$\frac{\partial \sigma_x}{\partial x} + \frac{\partial \sigma_{xy}}{\partial y} + \frac{\partial \sigma_{xz}}{\partial z} = f_x, \quad \frac{\partial \sigma_{xy}}{\partial x} + \frac{\partial \sigma_y}{\partial y} + \frac{\partial \sigma_{yz}}{\partial z} = f_y, \quad \frac{\partial \sigma_z}{\partial z} = -\bar{\rho}g + f_z, \tag{2.9}$$

where we make the assumption that

$$\frac{\partial \sigma_{xz}}{\partial x} + \frac{\partial \sigma_{yz}}{\partial y} = 0.$$

This assumption allows us to compute σ_z from (2.9) by simply imposing a Dirichlet condition on it at the basin's top (cf. Section 2.2.1).

Remark 2.1. *As is usual in poroelastic basins, we assume that the shear stresses within the water phase and between the water and solid phases are negligible with respect to those within the skeleton. Thus, in (2.7), the terms σ_{yz}, σ_{xz} and σ_{xy} are in fact the skeleton's shear stresses. This is not true of the normal stresses since the water pressure needs to be taken into account (cf. Section 3.1.1).*

2.1.3 Porosity

At this stage, we do not have an expression for the porosity ϕ, although it intervenes in many of the model equations, namely, (2.1), (2.2), (2.5) and (2.8). In a standard model for porous media, one could assume ϕ to be constant, which would close our model already. However, because of compaction, this is not satisfactory here. We derive a model for compaction, and thus ϕ, in Section 3.4.

2.2 Boundary and initial conditions

We suppose that the sedimentary top is given by the graph of a function s, that is, for all (x, y) the value $s(x, y)$ gives the vertical position of the top right above point (x, y, z), for any $z \leq s(x, y)$. Recall that the z-axis is directed upwards.

2.2.1 Boundary conditions

Integrating the third equation in (2.9) and (2.6) tells us to impose a total vertical stress and a temperature at the sedimentary top. Denoting by Ω the basin and by $\partial\Omega_{\text{top}}$ its top, i.e., $\partial\Omega_{\text{top}} = \{(x, y, z) \in \Omega \mid z = s(x, y)\}$, we impose

$$\begin{cases} \sigma_z(x, y, z) = p_{\text{sup}}(x, y) \\ T(x, y, z) = T_{\text{sup}}(x, y) \end{cases} \quad \text{for all } (x, y, z) \in \partial\Omega_{\text{top}} \text{ at all times.} \tag{2.10}$$

Here, p_{sup} is the pressure stemming from the weight of sea water and atmosphere lying above the basin. On the rest of the boundary $\partial\Omega$, we impose zero-flux conditions, i.e.,

$$\boldsymbol{V}_w \cdot \boldsymbol{\nu} = 0 \quad \text{on } \partial\Omega \setminus \partial\Omega_{\text{top}} \text{ at all times,}$$

where $\boldsymbol{\nu}$ is the outward unit normal of Ω.

Regarding stresses, note from (2.9) that these boundary conditions only close the problem for the vertical stress σ_z. Indeed, they do not give us the horizontal stresses σ_x and σ_y, nor do they give us the shear stresses σ_{yz}, σ_{xz} and σ_{xy}. Nevertheless, the horizontal stresses can be recovered from the vertical one whenever the horizontal strains are known and a constitutive stress-strain law is imposed (cf. Section 3.4.1). As to the shear stresses, they are not of interest to us in this paper since we suppose that they do not impact porosity (cf. Section 3.2.1); we therefore do not worry about closing the problem for them.

2.2.2 Initial conditions

The history of the basin is split into a sequence of geological episodes, called *events*, during which either a new layer of sediments is deposited or an old layer is eroded. We generically write t_0 the initial time of any *deposit* event.

Because each simulation starts at the beginning of a deposit event and layers are added to the top only, the initial conditions are already determined by the top boundary conditions given in (2.10):

$$\begin{cases} \sigma_z(t_0) = p_{\text{sup}}(t_0) \\ T(t_0) = T_{\text{sup}}(t_0) \end{cases} \quad \text{in new layer.}$$

3 Compaction

For the sake of presentation, we consider only one sedimentary layer starting from its initial time t_0 of deposition and eventually ending when fully eroded. Modeling the complete basin can then be achieved by applying the single-layer model in each layer.

As discussed in the introduction, we wish to integrate horizontal strains in a vertical porosity-stress law to account for horizontal compaction when oedometric conditions are not verified. We consider that the horizontal strains are known time-dependent parameters. The resulting model is what we refer to as simplified geomechanical model.

3.1 Relevant stress and strain tensors

We treat our basin as an *isotropic*, *poroelastic* material, thus undergoing *small* deformations. In this framework, the stress and strain quantities of relevance are the *effective* stress tensor and the *skeleton's infinitesimal* strain tensor.

3.1.1 Effective stress

Biot's theory [4] for consolidation couples fluid flow with rock deformation and introduces the effective stress tensor $\boldsymbol{\sigma}'$, which is defined as

$$\boldsymbol{\sigma}' = \boldsymbol{\sigma} - p_w \boldsymbol{b},$$

where $\boldsymbol{b}$ is Biot's tensor. In [5], the authors link Biot's tensor to the compressibility of the medium according to

$$\boldsymbol{b} = \left(1 - \frac{K_s}{K}\right) \boldsymbol{I} =: b\boldsymbol{I},$$

with K_s and K the moduli of compressibility of the solid phase and the skeleton, respectively, and $\boldsymbol{I}$ the identity matrix. Biot's coefficient b satisfies $b \simeq 1$ for a weakly compressible solid phase and a highly compressible skeleton, in which case we recover Terzaghi's theory for soil deformation [41]. For explicit expressions of b depending on porosity, we refer the reader to [7, 10, 30, 39].

The effective stress tensor reads

$$\boldsymbol{\sigma}' = \begin{pmatrix} \sigma'_x & \sigma_{xy} & \sigma_{xz} \\ \sigma_{xy} & \sigma'_y & \sigma_{yz} \\ \sigma_{xz} & \sigma_{yz} & \sigma'_z \end{pmatrix},$$

where $\sigma'_i = \sigma_i - p_w b$ for all $i \in \{x, y, z\}$. The tensor $\boldsymbol{\sigma}'$ is in fact the skeleton's stress tensor (cf. Remark 2.1).

Note that, by equilibrium with the sea water and the atmosphere, we have $p_w = p_{\text{sup}}$, that is, $\sigma'_z = \sigma_z - p_w b = (1-b)p_{\text{sup}}$ on the top boundary $\partial\Omega_{\text{top}}$; in particular, $\sigma'_z = 0$ on $\partial\Omega_{\text{top}}$ when $b = 1$. Equivalently, we have

$$\sigma'_z(t_0) = (1-b)p_{\text{sup}}(t_0); \tag{3.1}$$

in particular, $\sigma'_z(t_0) = 0$ when $b = 1$.

3.1.2 Skeleton's infinitesimal strain

We denote by $\boldsymbol{\varepsilon}$ the skeleton's infinitesimal strain, or deformation, tensor. (In the following, we omit the term "infinitesimal" when referring to $\boldsymbol{\varepsilon}$.) Because the basin is assumed to be elastic, $\boldsymbol{\varepsilon}$ coincides in fact with the elastic strain tensor and satisfies $|\boldsymbol{\varepsilon}| \ll 1$.

We use the following notation:

$$\boldsymbol{\varepsilon} = \begin{pmatrix} \varepsilon_x & \varepsilon_{xy} & \varepsilon_{xz} \\ \varepsilon_{xy} & \varepsilon_y & \varepsilon_{yz} \\ \varepsilon_{xz} & \varepsilon_{yz} & \varepsilon_z \end{pmatrix},$$

where ε_i and ε_{ij} are the normal and shear strains for all $i, j \in \{x, y, z\}$ with $i \neq j$. In agreement with our stress convention, any positive normal strain corresponds to a compression.

3.2 General compaction law

Given any differentiable time-dependent function f, we write $\dot{f}$ its time derivative, which we also refer to as the *rate* of f.

3.2.1 Generic formula

Compaction is characterized by a change in porosity under a change in compression. Supposing that the porosity rate does not depend on shear stresses (cf. Remark 2.1), we may let the porosity and effective stress tensor follow a law of the form

$$\dot{\phi} = \boldsymbol{F}(\phi, \boldsymbol{\sigma}'_{\mathrm{n}}) \cdot \dot{\boldsymbol{\sigma}}'_{\mathrm{n}}, \tag{3.2}$$

where $\boldsymbol{F}$ is a continuous, vector-valued function, $\boldsymbol{\sigma}'_{\mathrm{n}} := (\sigma'_x, \sigma'_y, \sigma'_z)$ is the diagonal vector of $\boldsymbol{\sigma}'$ and $\cdot$ stands for the Euclidean inner product. Following [39], we sometimes refer to $\boldsymbol{F}$ as the *elastoplastic* function, which, in particular, needs to keep the porosity between 0 and 1. If we were to treat chemical compaction in addition to mechanical compaction, then we would need to add a term of the form $\boldsymbol{G}(\phi, \boldsymbol{\sigma}'_{\mathrm{n}}) \cdot \boldsymbol{\sigma}'_{\mathrm{n}}$ to the right-hand side of (3.2) to account for viscoplastic effects [37–39]. Although the terminology just introduced involves the term "plastic", let us reiteratre that we do not consider plasticity in our model.

3.2.2 Porosity-free elastoplastic function

For simplicity, we assume that $\boldsymbol{F}$ only depends on effective stress:

$$\dot{\phi} = \boldsymbol{F}(\boldsymbol{\sigma}'_{\mathrm{n}}) \cdot \dot{\boldsymbol{\sigma}}'_{\mathrm{n}}. \tag{3.3}$$

We call (3.3) the *compaction law*, which is eventually nonlinear. We can retrieve an expression for ϕ by integrating it between the initial time t_0 and a time $t > t_0$:

$$\phi(t) = \phi(t_0) + \int_{t_0}^{t} \boldsymbol{F}(\boldsymbol{\sigma}'_{\mathrm{n}}(s)) \cdot \dot{\boldsymbol{\sigma}}'_{\mathrm{n}}(s)\, \mathrm{d}s. \tag{3.4}$$

This completes our standard basin model given in Section 2 provided we find an appropriate elastoplastic function $\boldsymbol{F}$. We first discuss the oedometric case and then generalize it to give our simplified geomechanical model.

3.3 Oedometric model

Assume in this section that we are within the oedometric hypothesis, that is, the strains satisfy

$$\varepsilon_x = \varepsilon_y = \varepsilon_{yz} = \varepsilon_{xz} = \varepsilon_{xy} = 0. \tag{3.5}$$

3.3.1 Vertical compaction law

Horizontal effects on porosity being negligible in this case, we choose $\boldsymbol{F}$ in (3.3) to depend exclusively on the vertical stress σ'_z:

$$\boldsymbol{F}(\boldsymbol{\sigma}'_{\mathrm{n}}) = (0, 0, -\beta(\sigma'_z)), \tag{3.6}$$

where β is a function determined by lithology, so that (3.3) becomes

$$\dot{\phi} = -\beta(\sigma'_z)\, \dot{\sigma}'_z. \tag{3.7}$$

This law is one-dimensional in that it only takes vertical stress into account.

3.3.2 Schneider's law

We choose Schneider's function for β [38]:

$$\beta(s) = \frac{\phi_1}{\sigma_1} e^{-s/\sigma_1} + \frac{\phi_2}{\sigma_2} e^{-s/\sigma_2}, \tag{3.8}$$

where $\phi_1, \phi_2 \geqslant 0$ (porosities) and $\sigma_1, \sigma_2 > 0$ (stresses) are known parameters depending on lithology. The compaction law (3.7) is thus referred to as *Schneider's law*. Let α be a primitive of $-\beta$, that is,

$$\alpha(s) = \phi_\mathrm{r} + \phi_1 e^{-s/\sigma_1} + \phi_2 e^{-s/\sigma_2}, \tag{3.9}$$

for some additional parameter ϕ_r called the residual porosity. At t_0, we impose

$$\phi(t_0) = \alpha(\sigma'_z(t_0)) = \phi_\mathrm{r} + \phi_1 e^{-(1-b)p_\mathrm{sup}(t_0)/\sigma_1} + \phi_2 e^{-(1-b)p_\mathrm{sup}(t_0)/\sigma_2}, \tag{3.10}$$

where we refer the reader to (3.1); this becomes $\phi(t_0) = \phi_\mathrm{r} + \phi_1 + \phi_2$ if $b = 1$. Then, (3.4) yields

$$\phi = \alpha(\sigma'_z). \tag{3.11}$$

When positive, the residual porosity helps numerically avoid the porosity to become negative as vertical effective stress increases.

Schneider's law is empirical and the parameters need to be found by experimental fitting; the double exponential formulation allows for a better fit at both upper and lower sediment layers. This is in contrast with the single-exponential law proposed by Athy [1], which is recovered when $\phi_2 = \phi_\mathrm{r} = 0$ in (3.8) and (3.9):

$$\beta(s) = \frac{\phi_1}{\sigma_1} e^{-s/\sigma_1} \quad \text{and} \quad \alpha(s) = \phi_1 e^{-s/\sigma_1}.$$

We refer the reader to [24] for an equivalent reformulation of Athy's law on permeability rather than porosity. Also, it is a fact that Athy's law can be derived as a solution to a partial differential equation when compaction happens fast [21].

3.3.3 Erosion

Schneider's law is adequate to describe compaction in oedometric conditions. It is less so if erosion is involved, i.e., if decompaction, eventually followed by recompaction, occurs. During erosion, the law in (3.8) can be adjusted to include decompaction and recompaction as elastic phenomena [38, 39]. We do not discuss this issue further and simply assume that (3.8) still holds for erosion.

3.4 Simplified geomechanical model

We now derive the compaction model to handle non-oedometric conditions. As already mentioned, we suppose that the horizontal strains ε_x and ε_y (and thus their rates $\dot{\varepsilon}_x$ and $\dot{\varepsilon}_y$) are known time-dependent functions.

3.4.1 Stress-strain constitutive law

We start by discussing the relationship between effective stress and strain (in fact, bewteen their rates).

Generic formula. We suppose that $\boldsymbol{\sigma}'$ and $\boldsymbol{\varepsilon}$ verify

$$\dot{\boldsymbol{\sigma}}' = \boldsymbol{G}(\boldsymbol{\sigma}', \varepsilon) : \dot{\varepsilon},$$

where $\boldsymbol{G}$ is a continuous function with fourth-order tensor values, called the *stiffness* tensor. This relation would need to be corrected according to finite strain theory using the spin tensor if we were to consider eventually large plastic strains [10, 16, 30]. Note that in classical infinitesimal elastic theory, $\boldsymbol{G}$ only depends on $\boldsymbol{\varepsilon}$ and so, by time integration, $\boldsymbol{\sigma}'$ is an explicit function of $\boldsymbol{\varepsilon}$; when furthermore the elasticity is linear, $\boldsymbol{G}$ is in fact independent of both $\boldsymbol{\sigma}'$ and $\boldsymbol{\varepsilon}$ and Hooke's law applies.

Strain-free stiffness tensor. Compaction impacts the form of the stiffness tensor $\boldsymbol{G}$. Indeed, as shown later (cf. (3.24)), assuming a compaction law of the form (3.3) requires $\boldsymbol{G}$ to depend on $\boldsymbol{\sigma}'$. In fact, in contrast with classical elasticity, we drop the dependence on $\boldsymbol{\varepsilon}$ and only keep that on $\boldsymbol{\sigma}'$:

$$\dot{\boldsymbol{\sigma}}' = \boldsymbol{G}(\boldsymbol{\sigma}') : \dot{\varepsilon}. \tag{3.12}$$

Equivalently, writing $\boldsymbol{H}(\boldsymbol{\sigma}') = \boldsymbol{G}(\boldsymbol{\sigma}')^{-1}$, we have

$$\dot{\varepsilon} = \boldsymbol{H}(\boldsymbol{\sigma}') : \dot{\boldsymbol{\sigma}}', \tag{3.13}$$

We call (3.12) and (3.13) the *stress-strain constitutive law*.

Hooke-type law. We choose Hooke's elastic law with stress-dependent Young modulus for the stiffness tensor, that is, we rewrite (3.12) as

$$\dot{\boldsymbol{\sigma}}' = \frac{E(\boldsymbol{\sigma}')}{1+\nu}\,\dot{\varepsilon} + \frac{\nu E(\boldsymbol{\sigma}')}{(1+\nu)(1-2\nu)}\,\mathrm{tr}(\dot{\varepsilon})\boldsymbol{I}, \tag{3.14}$$

where $\nu \in [0, 0.5)$ is Poisson's coefficient and $E > 0$ is Young's stress-dependent modulus. Equivalently, we rewrite (3.13) as

$$\dot{\varepsilon} = \frac{1+\nu}{E(\boldsymbol{\sigma}')}\,\dot{\boldsymbol{\sigma}}' - \frac{\nu}{E(\boldsymbol{\sigma}')}\,\mathrm{tr}(\dot{\boldsymbol{\sigma}}')\boldsymbol{I}, \tag{3.15}$$

For simplicity, we refer to both (3.14) and (3.15) as *Hooke's law*.

As a direct consequence of (3.15), we have

$$\mathrm{tr}(\dot{\varepsilon}) = \frac{1-2\nu}{E(\boldsymbol{\sigma}')}\,\mathrm{tr}(\dot{\boldsymbol{\sigma}}'). \tag{3.16}$$

The trace of $\dot{\varepsilon}$ is the *dilatation* or *relative volume change* of the skeleton. Also, from the first two equations in (3.15), we establish

$$\begin{aligned} \dot{\sigma}'_x &= \frac{\nu}{1-\nu}\,\dot{\sigma}'_z + \frac{E(\boldsymbol{\sigma}')}{1-\nu^2}(\dot{\varepsilon}_x + \nu\,\dot{\varepsilon}_y), \\ \dot{\sigma}'_y &= \frac{\nu}{1-\nu}\,\dot{\sigma}'_z + \frac{E(\boldsymbol{\sigma}')}{1-\nu^2}(\dot{\varepsilon}_y + \nu\,\dot{\varepsilon}_x), \end{aligned} \tag{3.17}$$

and so, summing these two equations and adding $\dot{\sigma}'_z$, we get

$$\mathrm{tr}(\dot{\boldsymbol{\sigma}}') = \frac{1+\nu}{1-\nu}\,\dot{\sigma}'_z + \frac{E(\boldsymbol{\sigma}')}{1-\nu}(\dot{\varepsilon}_x + \dot{\varepsilon}_y). \tag{3.18}$$

Initially, recalling (3.1), we impose

$$\sigma'_x(t_0) = \sigma'_y(t_0) = \frac{\nu}{1-\nu}\sigma'_z(t_0) = \frac{\nu}{1-\nu}(1-b)p_{\sup}(t_0), \tag{3.19}$$

which becomes $\sigma'_x(t_0) = \sigma'_y(t_0) = 0$ when $b = 1$.

Oedometric case. We briefly return to the oedometric case (cf. (3.5)).

Stress and strain tensors.—Both equations in (3.17) and (3.18) imply

$$\dot\sigma'_x = \dot\sigma'_y = \frac{\nu}{1-\nu}\,\dot\sigma'_z \quad \text{and} \quad \operatorname{tr}(\dot{\boldsymbol{\sigma}}') = \frac{1+\nu}{1-\nu}\,\dot\sigma'_z. \tag{3.20}$$

Thus, (3.16) gives

$$\dot\varepsilon_z = \operatorname{tr}(\dot{\boldsymbol{\varepsilon}}) = \frac{(1+\nu)(1-2\nu)}{(1-\nu)E(\boldsymbol{\sigma}')}\,\dot\sigma'_z. \tag{3.21}$$

Then, the oedometric rates of effective stress and strain tensors read as

$$\dot{\boldsymbol{\sigma}}' = \begin{pmatrix} \frac{\nu}{1-\nu} & 0 & 0 \\ 0 & \frac{\nu}{1-\nu} & 0 \\ 0 & 0 & 1 \end{pmatrix} \dot\sigma'_z \quad \text{and} \quad \dot{\boldsymbol{\varepsilon}} = \begin{pmatrix} 0 & 0 & 0 \\ 0 & 0 & 0 \\ 0 & 0 & \frac{(1+\nu)(1-2\nu)}{(1-\nu)E(\boldsymbol{\sigma}')} \end{pmatrix} \dot\sigma'_z. \tag{3.22}$$

Young's modulus.—To find an expression for Young's modulus, we use Schneider's law. Let us first note that, by solid incompressibility (cf. [36] for example),

$$\dot\phi = -(1-\phi)\operatorname{tr}(\dot{\boldsymbol{\varepsilon}}) = -(1-\phi)\,\dot\varepsilon_z. \tag{3.23}$$

Then, using (3.7), (3.11) and (3.21), we get

$$E(\boldsymbol{\sigma}') = \frac{(1+\nu)(1-2\nu)}{1-\nu}\,\frac{1-\alpha(\sigma'_z)}{\beta(\sigma'_z)}. \tag{3.24}$$

Thus, we see a posteriori, given the form of Schneider's function (3.8) and its primitive (3.11), that E must indeed depend on effective stress (specifically, on the vertical effective stress σ'_z), even under oedometric conditions.

Note also that the choice of taking Young's modulus as stress-dependent over Poisson's coefficient in (3.14) and (3.15) is arbitrary and is only motivated by the fact (3.24) is a simpler expression than its equivalent for ν.

3.4.2 Approximated problem

To determine the porosity, we introduce an *approximated problem* for the strains for which the oedometric hypothesis (3.5) holds and therefore Schneider's vertical law (3.7)-(3.8) is applicable.

More precisely, we take a stress-strain pair $(\boldsymbol{\sigma}^*, \boldsymbol{\varepsilon}^*)$ whose components verify

$$\varepsilon^*_x = \varepsilon^*_y = \varepsilon^*_{yz} = \varepsilon^*_{xz} = \varepsilon^*_{xy} = 0 \tag{3.25}$$

and

$$\sigma^*_i(t_0) = \sigma'_i(t_0) \quad \text{for all } i \in \{x, y, z\}, \tag{3.26}$$

where we refer the reader to (3.1) and (3.19).

Approximated porosity. Because of the oedometric hypothesis (3.25) being satisfied by the approximated strain tensor, Section 3.3 motivates the use of the following compaction law to define an approximated porosity ϕ^*:

$$\dot{\phi}^* = -\beta(\sigma_z^*)\,\dot{\sigma}_z^*, \tag{3.27}$$

where β is given by Schneider's function (3.8). We further require that

$$\phi^*(t_0) = \phi(t_0), \tag{3.28}$$

with $\phi(t_0)$ given in (3.10).

Approximated tensors. We let $\boldsymbol{\sigma}^*$ and $\boldsymbol{\varepsilon}^*$ satisfy the constitutive relation

$$\dot{\boldsymbol{\varepsilon}}^* = \boldsymbol{H}(\boldsymbol{\sigma}^*) : \dot{\boldsymbol{\sigma}}^*,$$

where we recall that $\boldsymbol{H}$ is given by (3.15). We directly get the analogue of (3.16):

$$\operatorname{tr}(\dot{\boldsymbol{\varepsilon}}^*) = \frac{1-2\nu}{E(\boldsymbol{\sigma}^*)} \operatorname{tr}(\dot{\boldsymbol{\sigma}}^*).$$

Also, following the computations in Section 3.4.1, we yield

$$\dot{\sigma}_x^* = \dot{\sigma}_y^* = \frac{\nu}{1-\nu}\,\dot{\sigma}_z^*, \tag{3.29}$$

and

$$\operatorname{tr}(\dot{\boldsymbol{\sigma}}^*) = \frac{1+\nu}{1-\nu}\,\dot{\sigma}_z^*, \tag{3.30}$$

in agreement with the oedometric forms given in (3.20).

Approximating assumption. The assumption we wish to make is that the approximated porosity ϕ^* is close to the *actual* porosity ϕ, that is,

$$\left|\phi^* - \phi\right| \ll 1, \tag{3.31}$$

so that ϕ can be replaced by ϕ^* wherever needed. Thanks to (3.28), this is equivalent to

$$\delta := \left|\dot{\phi}^* - \dot{\phi}\right| \ll 1. \tag{3.32}$$

For this approximation to be justified given (3.7) and (3.27), we still need to choose an appropriate vertical approximated stress σ_z^*.

Vertical approximated stress. To account for the horizontal effects of compaction, σ_z^* must include the horizontal deformations ε_x and ε_y. Moreover, for consistency, it should coincide with σ_z' in oedometric conditions.

Convex combination.—We ask for a convex combination of rates of horizontal stresses to be preserved, that is, for some $\lambda \in [0,1]$ we let

$$(1-\lambda)\,\dot{\sigma}_x^* + \lambda\,\dot{\sigma}_y^* = (1-\lambda)\,\dot{\sigma}_x' + \lambda\,\dot{\sigma}_y'. \tag{3.33}$$

Given (3.17) and (3.29), this yields

$$\frac{\nu}{1-\nu}\,\dot{\sigma}_z^* = \frac{\nu}{1-\nu}\,\dot{\sigma}_z' + \frac{E(\boldsymbol{\sigma}')}{1-\nu^2}\left(\left((1-\lambda)+\nu\lambda\right)\dot{\varepsilon}_x + \left(\lambda+\nu(1-\lambda)\right)\dot{\varepsilon}_y\right),$$

where we recall that $E(\boldsymbol{\sigma}')$ is Young's stress-dependent modulus. Then,

$$\dot{\sigma}_z^* = \dot{\sigma}_z' + \frac{E(\boldsymbol{\sigma}')}{\nu(1+\nu)} \left(\dot{\varepsilon}_x + \dot{\varepsilon}_y - (1-\nu)(\lambda\, \dot{\varepsilon}_x + (1-\lambda)\, \dot{\varepsilon}_y)\right). \tag{3.34}$$

The choice for the parameter λ is arbitrary at this point. We impose that only the rate of x-stress should be preserved (i.e., $\lambda = 0$) if only the rate of x-strain is nonzero and vice-versa (i.e., $\lambda = 1$) if only the rate of y-strain is nonzero. Therefore, we choose

$$\lambda = \frac{\left|\dot{\varepsilon}_y\right|}{\left|\dot{\varepsilon}_x\right| + \left|\dot{\varepsilon}_y\right|},$$

and (3.34) becomes

$$\dot{\sigma}_z^* = \dot{\sigma}_z' + \frac{E(\boldsymbol{\sigma}')}{\nu(1+\nu)} \begin{cases} \left(\dot{\varepsilon}_x + \dot{\varepsilon}_y - \dfrac{2(1-\nu)\, \dot{\varepsilon}_x \dot{\varepsilon}_y}{\dot{\varepsilon}_x + \dot{\varepsilon}_y}\right) & \text{if } \dot{\varepsilon}_x \dot{\varepsilon}_y > 0, \\ (\dot{\varepsilon}_x + \dot{\varepsilon}_y) & \text{if } \dot{\varepsilon}_x \dot{\varepsilon}_y \leqslant 0. \end{cases} \tag{3.35}$$

Remark 3.1. *In oedometric conditions, we note that* $\dot{\sigma}_z^* = \dot{\sigma}_z'$ *and, thanks to* (3.26)*, that* $\sigma_z^* = \sigma_z'$*; furthermore,* (3.7) *and* (3.27) *give* $\phi^* = \phi$*.*

Other possible choices.— There are various viable conditions to impose other than (3.33). For example, we could preserve the stress trace:

$$\operatorname{tr}(\dot{\boldsymbol{\sigma}}^*) = \operatorname{tr}(\dot{\boldsymbol{\sigma}}'), \tag{3.36}$$

which, thanks to (3.18) and (3.30), would lead to

$$\dot{\sigma}_z^* = \dot{\sigma}_z' + \frac{E(\boldsymbol{\sigma}')}{1+\nu}(\dot{\varepsilon}_x + \dot{\varepsilon}_y).$$

This relation, as opposed to our choice (3.35), disregards completely the relative magnitude of the horizontal-strain rates. Interestingly, though, thanks to (3.30) and (3.36), we have $E(\boldsymbol{\sigma}')\operatorname{tr}(\boldsymbol{\varepsilon}) = E(\boldsymbol{\sigma}^*)\operatorname{tr}(\boldsymbol{\varepsilon}^*)$, where $\operatorname{tr}(\boldsymbol{\varepsilon})$ and $\operatorname{tr}(\boldsymbol{\varepsilon}^*)$ are the relative volume changes for the actual and approximated problems, respectively.

In view of the above discussion, we note that a general expression for the rate of vertical approximated stress is the following *additive* adjustment of the rate of vertical effective stress:

$$\dot{\sigma}_z^* = \dot{\sigma}_z' + \zeta(\dot{\varepsilon}_x, \dot{\varepsilon}_y) E(\boldsymbol{\sigma}'), \tag{3.37}$$

for some strain-dependent, continuous function ζ such that $\zeta(0,0) = 0$. For instance, in our case (cf. (3.35)), we have

$$\zeta(\dot{\varepsilon}_x, \dot{\varepsilon}_y) = \frac{1}{\nu(1+\nu)} \begin{cases} \left(\dot{\varepsilon}_x + \dot{\varepsilon}_y - \dfrac{2(1-\nu)\, \dot{\varepsilon}_x \dot{\varepsilon}_y}{\dot{\varepsilon}_x + \dot{\varepsilon}_y}\right) & \text{if } \dot{\varepsilon}_x \dot{\varepsilon}_y > 0, \\ (\dot{\varepsilon}_x + \dot{\varepsilon}_y) & \text{if } \dot{\varepsilon}_x \dot{\varepsilon}_y \leqslant 0. \end{cases} \tag{3.38}$$

One could also integrate geometrical constraints related to the basin's shape into the function ζ. We leave the detailed study of the many possible choices of ζ to a future work.

Young's modulus. To close our approximated problem, and therefore our simplified geomechanical model given by (3.27)-(3.31)-(3.35), we need to determine an expression for Young's stress-dependent modulus. To this end, we split oedometric and non-oedometric contributions in porosity, effective stress and strain.

Porosity.—We split the elastoplastic function $\boldsymbol{F}$ in the compaction law (3.3) according to

$$\boldsymbol{F} = \boldsymbol{F}_{\mathrm{o}} + \boldsymbol{F}_{\mathrm{no}}, \tag{3.39}$$

where $\boldsymbol{F}_{\mathrm{o}}$ follows the oedometric formulation given in (3.6), that is,

$$\boldsymbol{F}_{\mathrm{o}}(\boldsymbol{\sigma}'_{\mathrm{n}}) = (0, 0, -\beta(\sigma'_z)). \tag{3.40}$$

This leads to a decomposition of the porosity as

$$\phi = \phi_{\mathrm{o}} + \phi_{\mathrm{no}}, \tag{3.41}$$

where ϕ_{o} and ϕ_{no} satisfy $\dot{\phi}_{\mathrm{o}} = \boldsymbol{F}_{\mathrm{o}}(\boldsymbol{\sigma}'_{\mathrm{n}}) \cdot \dot{\boldsymbol{\sigma}}'_{\mathrm{n}}$ and $\dot{\phi}_{\mathrm{no}} = \boldsymbol{F}_{\mathrm{no}}(\boldsymbol{\sigma}'_{\mathrm{n}}) \cdot \dot{\boldsymbol{\sigma}}'_{\mathrm{n}}$ and are the oedometric and non-oedometric contributions to the porosity change $\dot{\phi}$; in particular, there holds

$$\dot{\phi}_{\mathrm{o}} = -\beta(\sigma'_z)\, \dot{\sigma}'_z,$$

where β is Schneider's function (3.8).

Effective stress and strain.—Similarly as for the porosity, we split the effective stress and strain tensors as

$$\boldsymbol{\sigma}' = \boldsymbol{\sigma}'_{\mathrm{o}} + \boldsymbol{\sigma}'_{\mathrm{no}} \quad \text{and} \quad \boldsymbol{\varepsilon} = \boldsymbol{\varepsilon}_{\mathrm{o}} + \boldsymbol{\varepsilon}_{\mathrm{no}},$$

where, according to the stress-strain constitutive law (3.13), we have

$$\dot{\boldsymbol{\varepsilon}}_{\mathrm{o}} = \boldsymbol{H}(\boldsymbol{\sigma}') : \dot{\boldsymbol{\sigma}}'_{\mathrm{o}} \quad \text{and} \quad \dot{\boldsymbol{\varepsilon}}_{\mathrm{no}} = \boldsymbol{H}(\boldsymbol{\sigma}') : \dot{\boldsymbol{\sigma}}'_{\mathrm{no}}, \tag{3.42}$$

with $\boldsymbol{H}$ given in (3.15). From (3.17) and (3.22), we choose

$$\dot{\boldsymbol{\sigma}}'_{\mathrm{o}} = \begin{pmatrix} \frac{\nu}{1-\nu} & 0 & 0 \\ 0 & \frac{\nu}{1-\nu} & 0 \\ 0 & 0 & 1 \end{pmatrix} \dot{\sigma}'_z. \tag{3.43}$$

From (3.42) and (3.43), we get

$$\operatorname{tr}(\dot{\boldsymbol{\varepsilon}}_{\mathrm{o}}) = \frac{(1+\nu)(1-2\nu)}{(1-\nu)E(\boldsymbol{\sigma}')}\, \dot{\sigma}'_z. \tag{3.44}$$

Stress-dependent modulus.—From (3.23), there holds

$$\dot{\phi} = -(1-\phi)\operatorname{tr}(\dot{\boldsymbol{\varepsilon}}) = -(1-\phi)\operatorname{tr}(\dot{\boldsymbol{\varepsilon}}_{\mathrm{o}}) - (1-\phi)\operatorname{tr}(\dot{\boldsymbol{\varepsilon}}_{\mathrm{no}}).$$

By identification with (3.41), we therefore find that $\dot{\phi}_{\mathrm{o}}$ and $\operatorname{tr}(\dot{\boldsymbol{\varepsilon}}_{\mathrm{o}})$ satisfy

$$\dot{\phi}_{\mathrm{o}} = -(1-\phi)\operatorname{tr}(\dot{\boldsymbol{\varepsilon}}_{\mathrm{o}}). \tag{3.45}$$

Then, (3.44) and (3.45) lead to

$$E(\boldsymbol{\sigma}') = \frac{(1+\nu)(1-2\nu)}{1-\nu} \frac{1-\phi}{\beta(\sigma'_z)}. \tag{3.46}$$

Our simplified geomechanical model for compaction is therefore finally given by (3.27)-(3.31)-(3.35)-(3.46), summarized by

$$\begin{cases} \phi = \phi^*, \\ \dot{\phi}^* = -\beta(\sigma_z^*)\,\dot{\sigma}_z^*, \\ \dot{\sigma}_z^* = \dot{\sigma}_z' + \dfrac{E(\boldsymbol{\sigma}')}{\nu(1+\nu)} \begin{cases} \left(\dot{\varepsilon}_x + \dot{\varepsilon}_y - \dfrac{2(1-\nu)\,\dot{\varepsilon}_x\dot{\varepsilon}_y}{\dot{\varepsilon}_x + \dot{\varepsilon}_y}\right) & \text{if } \dot{\varepsilon}_x\dot{\varepsilon}_y > 0, \\ (\dot{\varepsilon}_x + \dot{\varepsilon}_y) & \text{if } \dot{\varepsilon}_x\dot{\varepsilon}_y \leqslant 0, \end{cases} \\ E(\boldsymbol{\sigma}') = \dfrac{(1+\nu)(1-2\nu)}{1-\nu}\dfrac{1-\phi}{\beta(\sigma_z')}. \end{cases} \tag{3.47}$$

Validity of the model. Let us come back to the question of the validity of the assumption that $\phi^* = \phi$ (cf. (3.31) and (3.32)). When there are no horizontal strains, we already know from Remark 3.1 that our model is such that $\dot{\phi}^* = \dot{\phi}$ and so $\delta = 0$ (cf. (3.32)). However, we would like to *quantify* how small $\dot{\varepsilon}_x$ and $\dot{\varepsilon}_y$ need to be for δ to be reasonably small and thus our model to be valid. Answering this question requires the use of advanced analytical tools, which is out of the scope of this paper. Instead, we validate our model numerically on a complex test case in Section 4.

Still, to give an idea on how to answer the question analytically, we give a formal computation in this direction. We have

$$\begin{aligned} \delta &= \left|\boldsymbol{F}(\boldsymbol{\sigma}_{\mathrm{n}}') \cdot \dot{\boldsymbol{\sigma}}_{\mathrm{n}}' + \beta(\sigma_z^*)\,\dot{\sigma}_z^*\right| \\ &\leqslant \left|(\boldsymbol{F}_{\mathrm{no}}(\boldsymbol{\sigma}_{\mathrm{n}}') + (0,0,\beta(\sigma_z^*) - \beta(\sigma_z'))) \cdot \dot{\boldsymbol{\sigma}}_{\mathrm{n}}'\right| + \beta(\sigma_z^*)\left|\dot{\sigma}_z^* - \dot{\sigma}_z'\right| \\ &\leqslant \left|\boldsymbol{F}_{\mathrm{no}}(\boldsymbol{\sigma}_{\mathrm{n}}') \cdot \dot{\boldsymbol{\sigma}}_{\mathrm{n}}'\right| + \left|\beta(\sigma_z^*) - \beta(\sigma_z')\right|\left|\dot{\sigma}_z'\right| + \beta(\sigma_z^*)E(\boldsymbol{\sigma}')\left|\zeta(\dot{\varepsilon}_x, \dot{\varepsilon}_y)\right| \\ &\leqslant \left|\boldsymbol{F}_{\mathrm{no}}(\boldsymbol{\sigma}_{\mathrm{n}}') \cdot \dot{\boldsymbol{\sigma}}_{\mathrm{n}}'\right| + \left|\beta(\sigma_z^*) - \beta(\sigma_z')\right|\left|\dot{\sigma}_z'\right| + \frac{(1+\nu)(1-2\nu)}{1-\nu}\frac{\beta(\sigma_z^*)}{\beta(\sigma_z')}\left|\zeta(\dot{\varepsilon}_x, \dot{\varepsilon}_y)\right|, \end{aligned}$$

where the first line comes from (3.3) and (3.27), the second line from (3.39) and (3.40), the third line from (3.37) and the fourth line from (3.46) and the fact that $\phi < 1$. Recall that ζ is given by (3.38) in our case. We thus see that if we have a control on how close $\beta(\sigma_z^*)$ is to $\beta(\sigma_z')$, then the second and third terms in the right-hand side of the last inequality can be bounded by $|\dot{\sigma}_z'|$, $|\dot{\varepsilon}_x|$ and $|\dot{\varepsilon}_y|$. The first term, however, depends on the non-oedometric contribution to the porosity, on which we do not have any information. Hence, for the moment, this analysis is inconclusive.

4 Simulations

We now discuss the numerical results obtained with our simplified geomechanical model (3.47) for compaction coded entirely in ArcTem.

4.1 Neuquén basin

We test our model on the Vaca Muerta formation of the Neuquén basin in Argentina. Its geological history involves many episodes of tectonic and sedimentary deformation, which makes it an attractive site to test compaction models.

We subdivide the basin's history into 30 events starting at −200 My and ending at the present day. These events include the deposition of sediments such as sandstone and carbonates over the first 20 events and their erosion at the top of the basin in the last 10 events. We use the same geometrical, lithological and mechanical parameters as in [3] and validate our results by comparison with those obtained there using the code A^2 in combination with the compaction model derived in [25]. We refer the reader to [3] for a detailed account of the basin's history and sediments' properties; importantly, the basin shows drained conditions with hydrostatic pressure in the upper layers, in contrast with the lower layers.

The main characteristics of the basin, summarized in Figure 1, are as follows:

- Spatial dimensions: 195 km East-West and 180 km North-South
- Spatial discretization: 100 620 finite-volume cells
- Sediments: 7 groups of different materials
- East-West strain: 4 % from −10 My to −8 My (2 events) and 2 % from −8 My to present day (8 events)

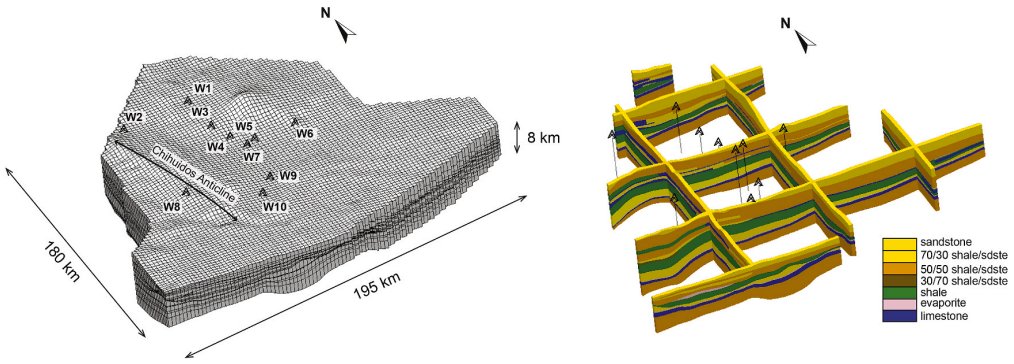

(a) Representation of the mesh with a five-time vertical exaggeration (left); several longitudinal and transversal sections of the basin colored by sediment groups (right)

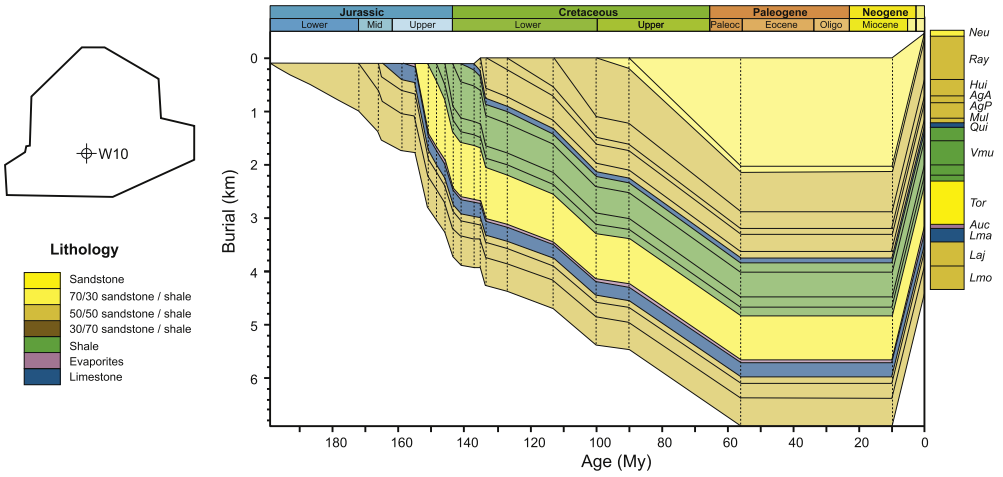

(b) Lithology and burial evolution of each sedimentary group during the Mesozoic and Cenozoic eras at Well 10 (W10)

Figure 1: Geometrical and lithological model of the Neuquén basin (from [25])

4.2 Parameters

We give in Table 1 the parameters chosen for our simulations and involved in the model equations given through Sections 2 and 3. As already mentioned, these parameters coincide with those used in [3].

	parameter	value (or interval of)	unit
densities	$\rho_{s,0}$	$[2645, 2710]$	$\mathrm{kg \cdot m^{-3}}$
	$\rho_{w,0}$	3620	$\mathrm{kg \cdot m^{-3}}$
	α_w	3.9×10^{-4}	$\mathrm{°C^{-1}}$
	β_w	4.5×10^{-4}	$\mathrm{MPa^{-1}}$
	T_0	15	°C
	P_0	0.1	MPa
water mobility	a_w	21.5	$\mathrm{Pa \cdot s \cdot °C^{-1}}$
	b_w	8078	$\mathrm{°C^2}$
	c_w	1200	°C
permeability	S_0	$[1.7 \times 10^{12}, 5 \times 10^{7}]$	$\mathrm{m^2}$
	ϕ_0	0.1	%
	k_1	20	–
	k_2	0.2	–
	n_1	5	–
	n_2	3	–
	m_1, m_2	2	–
geothermal gradient	G	$[0.046, 0.068]$	$\mathrm{°C \cdot m^{-1}}$
external force	$\boldsymbol{f}$	$(0, 0, 0)$	$\mathrm{kg \cdot m^{-2} \cdot s^{-2}}$
boundary conditions	p_{sup}	0.1	MPa
	T_{sup}	$[18, 26]$	°C
Biot's coefficient	b	1	–
Schneider's law	ϕ_{r}	$[0.01, 0.04]$	%
	ϕ_1	$[0.29, 0.56]$	%
	ϕ_2	0	%
	σ_1	$[1.6, 40]$	MPa
	σ_2	10	MPa
Poisson's coefficient	ν	0.24	–

Table 1: Chosen parameters of the model equations

In addition, the horizontal strain rates, measured in $\mathrm{s^{-1}}$, are of the form

$$\dot{\varepsilon}_i = \begin{cases} 0, & t < -10\,\mathrm{My}, \\ \alpha_i, & -10\,\mathrm{My} \leqslant t < -8\,\mathrm{My}, \\ \beta_i, & -8\,\mathrm{My} \leqslant t, \end{cases}$$

where, for $i \in \{x, y\}$, the parameters α_i and β_i are selected from the list below:

(zero) $\alpha_x = \beta_x = \alpha_y = \beta_y = 0$.

(ref) $\alpha_x = 0.02$, $\beta_x = 0.0025$ and $\alpha_y = \beta_y = 0$.

(dble) $\alpha_x = 0.04$, $\beta_x = 0.005$ and $\alpha_y = \beta_y = 0$.

(xy) $\alpha_x = \alpha_y = 0.01$ and $\beta_x = \beta_y = 0.00125$.

(neg) $\alpha_x = -0.0025$, $\beta_x = -0.0003125$ and $\alpha_y = \beta_y = 0$.

Choice **(zero)** refers to oedometric conditions, where lateral deformations are neglected. Choice **(ref)** corresponds to that in [3] and to experimentally observed data (cf. Section 4.1), and thus gives us a reference point for our simulations.

4.3 Results

We first compare the results of our simulations with those given in [3] using A^2, where we make use of **(zero)**, **(ref)** and **(dble)**. Then, we show additional results where the horizontal strains follow **(xy)** and **(neg)**. All the results are given at the present day, i.e., at the end of the simulations. Finally, we give the CPU time for each simulation.

4.3.1 Comparison with [3]

Figure 2 compares our results with [3] (A^2) under the reference strains **(ref)** along Well 10 (W10); there, we display the horizontal total stresses, the water pressure and the porosity. We also show experimental data points for the pressure and the porosity under this same condition **(ref)** and give the respective results when no horizontal strains are imposed, i.e., when the oedometric condition **(zero)** holds. We see that our porosity stays very close in the lower layers to that obtained with A^2. In the upper layers, the porosities diverge slightly but both stay within the data cloud. The results are not as positive for the horizontal stresses and the pressure; indeed, although the trends are very similar to those with A^2, the values gradually separate as depth increases. Still, there is a significant improvement when switching from **(zero)** to **(ref)**, in particular for the porosity, which shows that our simplified model does account for horizontal effects and is an improvement compared to an oedometric model, as desired, albeit underestimating the horizontal stresses and the pressure.

Because our model seems to underestimate horizontal stresses and pressure, we present in Figure 3 our results along W10 when the strain condition **(dble)** holds, i.e., when the horizontal strains are doubled with respect to the reference ones **(ref)**. The results are still showing underestimated values of the horizontal stresses and the pressure, although less significantly and in deeper layers (compare Figures 2 and 3). There is also a compelling improvement for the porosity, which is now closer to the A^2 result and more centered within the data points.

In Figure 4, we reproduce the profile obtained in [3] of the overpressure (i.e., the difference between the water pressure and the hydrostatic pressure) at the bottom of the basin and over a cross-section at the center of the basin. It shows both results when no horizontal deformations and when reference horizontal deformations are

applied. Figure 5 presents our results for comparison with Figure 4. Again, in accordance with Figures 2 and 3, we see that we underestimate the overpressure under the strain condition **(ref)** and get much closer to the A^2 results when **(dble)** holds instead.

The noted underestimating behavior should not diminish the fact that the results given under **(ref)** and **(dble)** still show great improvement compared to the oedometric simulation **(zero)**, in particular for the overpressure, pressure and porosity in the undrained region of the basin, i.e., in the deep layers.

4.3.2 Additional results

To illustrate the flexibility of our simplified model, Figure 6 shows the horizontal stresses, the pressure and the porosity along W10 when the horizontal strains are spread evenly in the x- and y-directions (cf. **(xy)**) and when negative horizontal strains are applied (cf. **(neg)**), i.e., when there is a horizontal extension rather than a compression. As expected, the condition **(xy)** yields higher horizontal stresses and pressure and lower porosity than **(zero)**, whereas the condition **(neg)** yields similar horizontal stresses and pressure and higher porosity. Note that, although the total horizontal strain in **(xy)** is the same as in **(ref)**, the results are different (compare Figures 2 and 6); this illustrates that our simplified model takes the direction of the strains into account when they are positive (cf. (3.35)).

When running simulations with **(neg)**, we identified a limitation of our approach. Namely, when the horizontal extension is large, the pressure locally becomes very small while the porosity becomes very large, which prevents the simulation from converging. We were not able to impose any extension stronger than that given in **(neg)**.

4.3.3 CPU times

Table 2 lists the CPU times required to run our simulations. We note that the difference in CPU time between a purely vertical model (i.e., an oedometric model, where no horizontal deformations are taken into account) and our simplified model goes from 24.9 % to 61.6 %, depending on the magnitude of the horizontal strains. This is a very attractive feature given that for a full-dimensional, finite-element approach, as used in [3], the computational time loss in comparison to an oedometric model is much higher.

	Time [min]
(zero)	55.8
(ref)	80.8
(dble)	90.2
(xy)	77.2
(neg)	69.7

Table 2: CPU time for each simulation run

5 Conclusion and outlook

The model proposed in this paper to describe mechanical compaction is based on an alteration of Schneider's vertical porosity-stress law and an elastic stress-strain

constitutive law involving a stress-dependent Young modulus. It coincides with classical modeling in oedometric conditions and provides a computation of porosity in non-oedometric conditions which is simpler, although not as accurate, compared to a full-dimensional, elastoplastic model. On the test case given by the Neuquén basin, our simplified model, coded in the finite-volume simulator ArcTem, shows reasonable accuracy in pressure, porosity and vertical stress along a drilling well, as well as in overpressure at the bottom and over a vertical cross-section at the center of the basin. Overall, our model tends to underestimate the horizontal stresses, the pressure and the overpressure. Still, it shows significant improvement compared to an oedometric model, in particular in the lower, undrained compartment of the basin, and it produces very advantageous computational times. Therefore, it may offer a quick way to get pre-validating results before spending the time and computational resources required by a three-dimensional, finite-element simulator.

Although the model shows promising first results, it would still benefit from further numerical validation by comparing results on different wells, cross-sections and test cases altogether. From the modeling and analytical point of view, other choices of approximated stresses need to be investigated, i.e., other functions ζ in (3.37) need to be tested; also, the analytical validation of the model requires additional work to show that the approximated porosity is indeed close to the actual one for a given range of horizontal stresses and strains (cf. the computation at the end of Section 3.4.2).

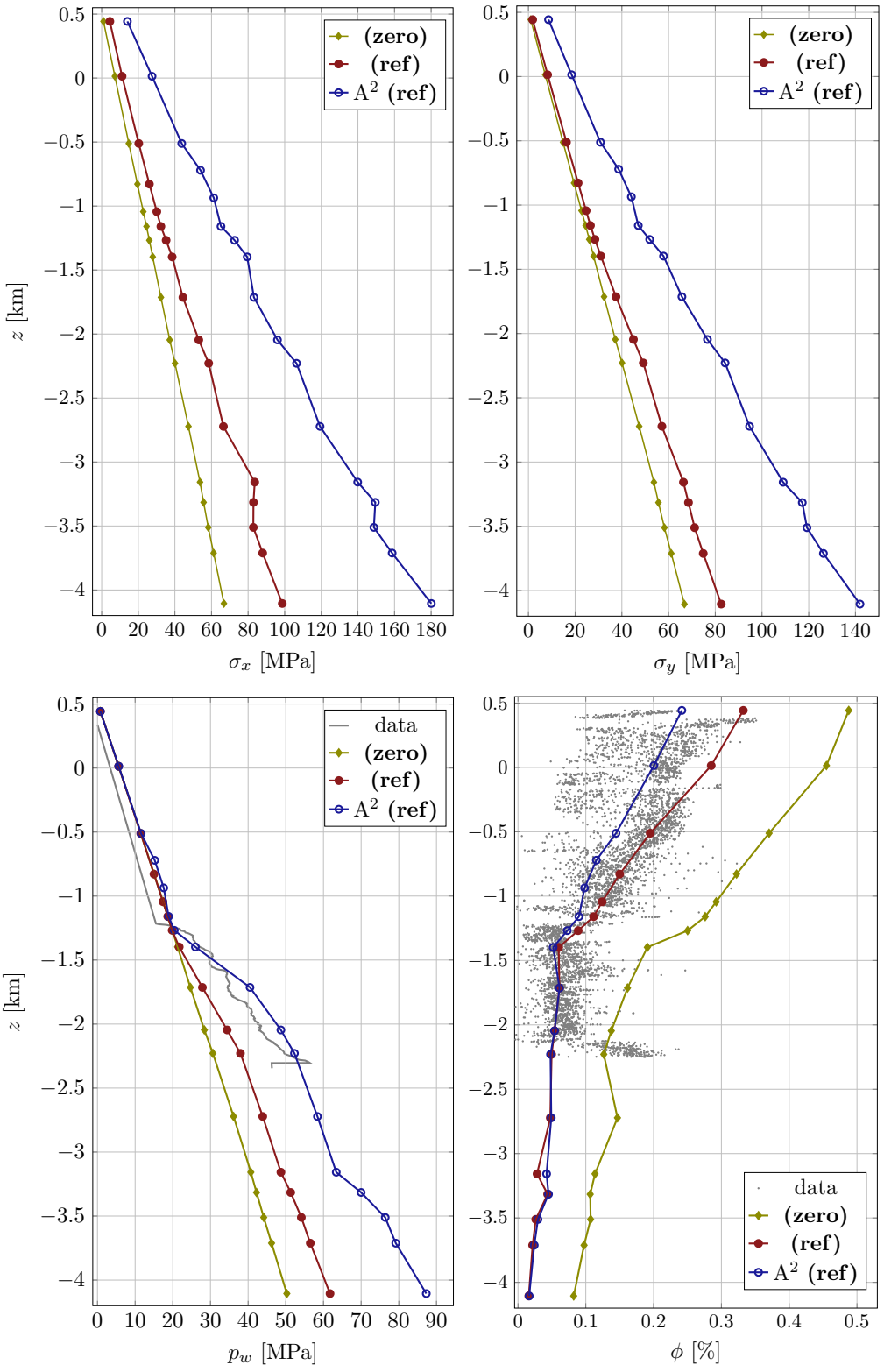

Figure 2: Comparison with A^2 under the strain condition **(ref)** and results under **(zero)** along W10 (data points and A^2 results from [3])

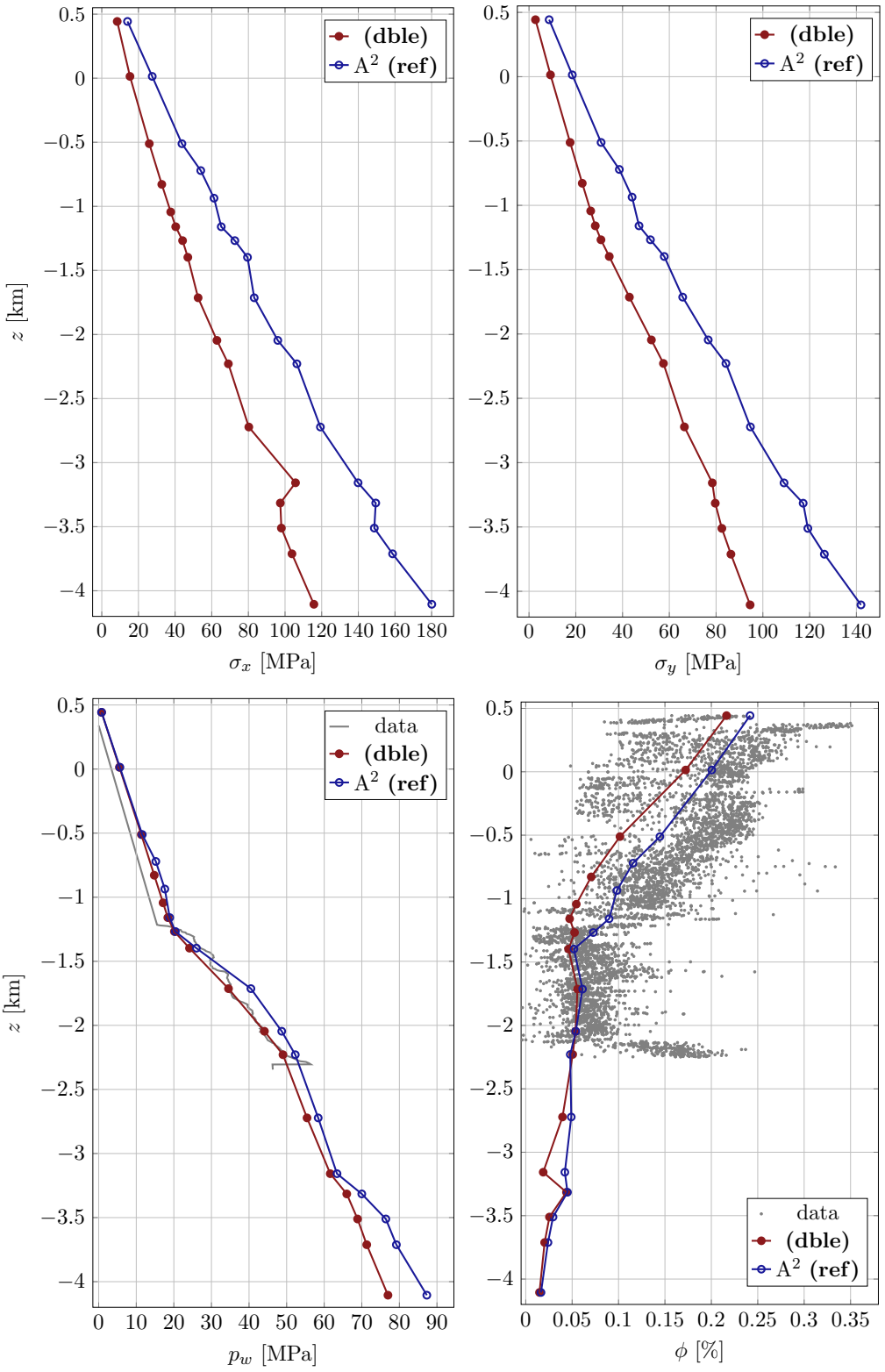

Figure 3: Results under the strain condition **(dble)** along W10 and comparison with A^2 (data points and A^2 results from [3])

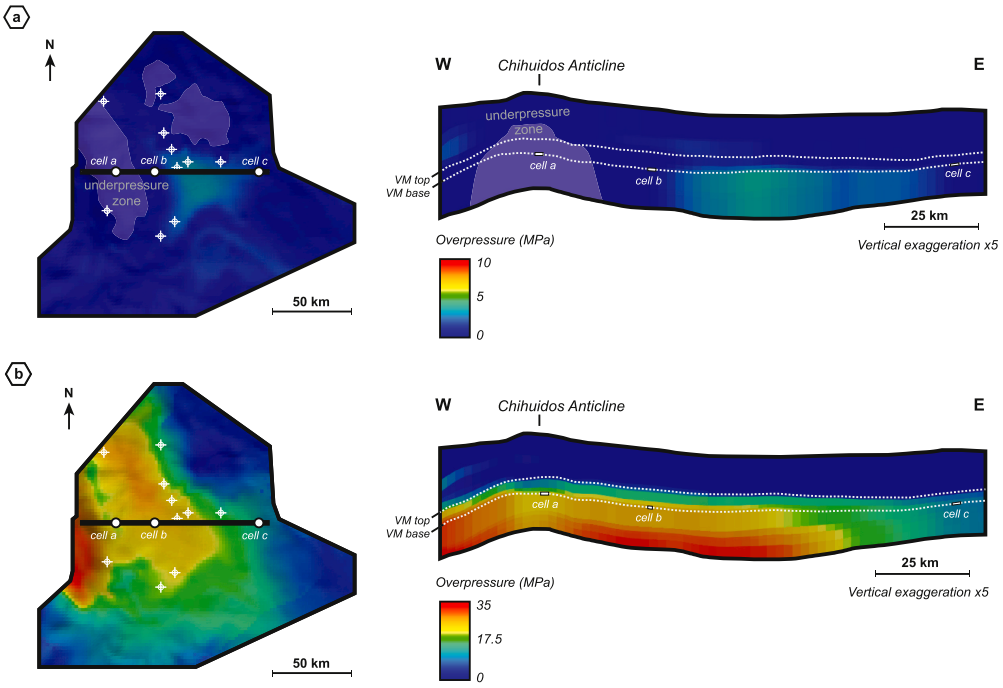

Figure 4: A^2 overpressure at bottom and over central cross-section under no horizontal strains (top) and reference horizontal strains (bottom) (from [3])

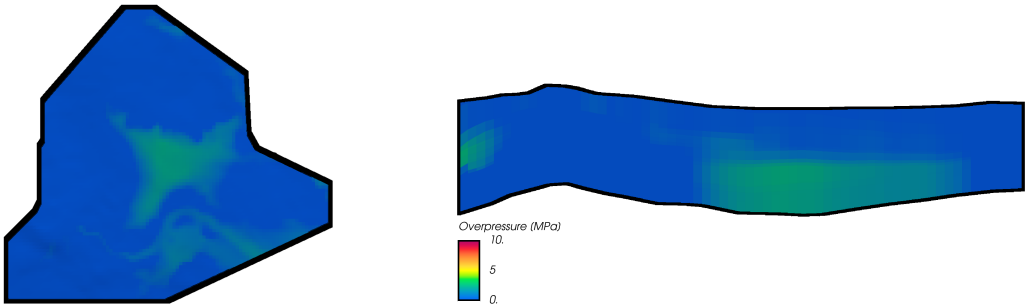

(a) **(zero)**

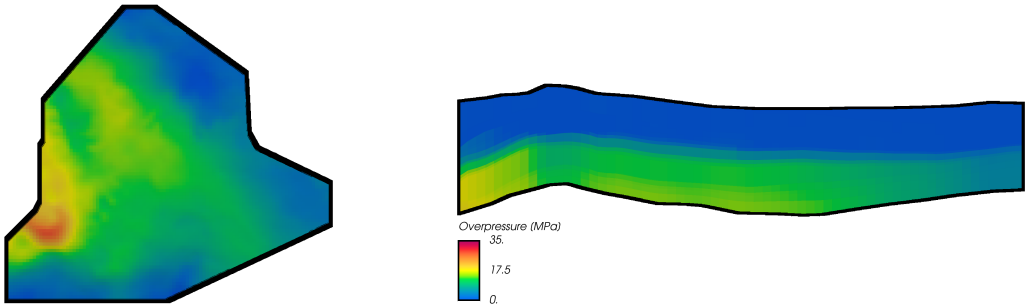

(b) **(ref)**

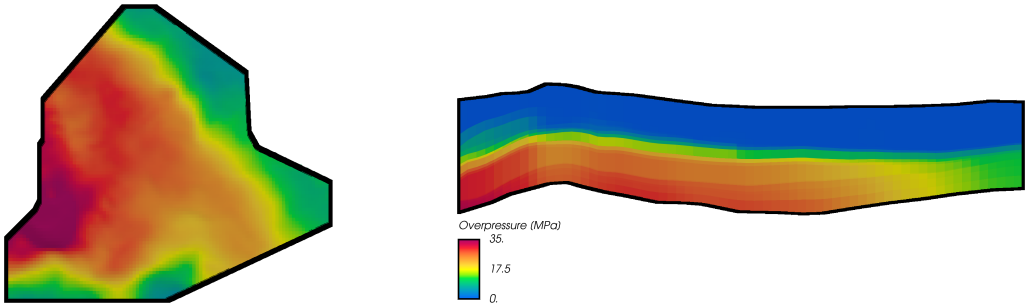

(c) **(dble)**

Figure 5: Overpressure at bottom and over central cross-section under the strain conditions **(zero)**, **(ref)** and **(dble)**

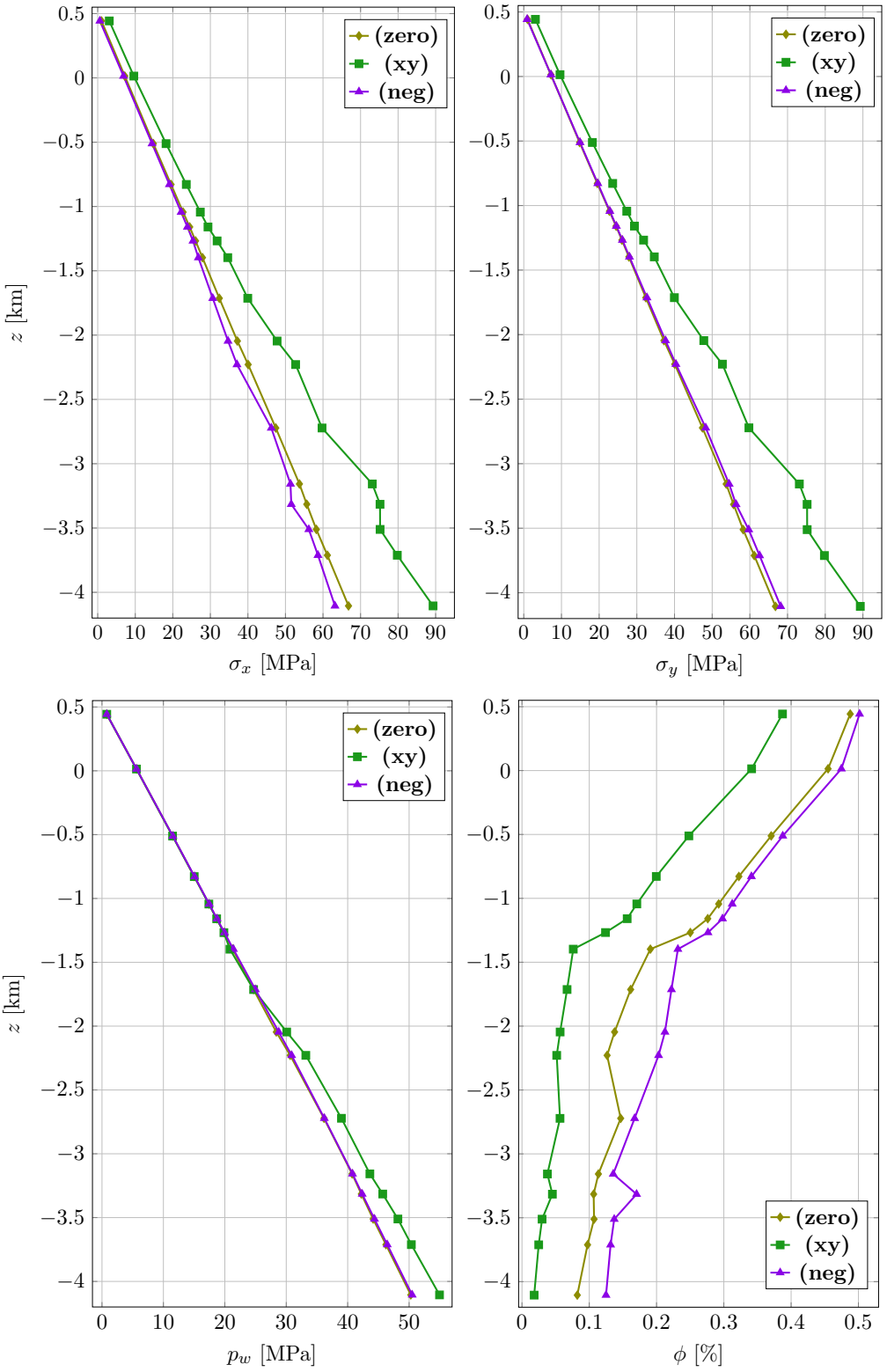

Figure 6: Results along W10 under the strain conditions **(zero)**, **(xy)** and **(neg)**

Acknowledgments

We thank the authors of [3] for sharing the A^2 data that made the validation of our model possible. This research did not receive any specific grant from funding agencies in the public, commercial, or not-for-profit sectors.

References

[1] L. F. Athy. Density, porosity, and compaction of sedimentary rocks. *AAPG Bulletin*, 14(1):1–24, 1930.

[2] A. Beall and A. Fisher. Sedimentology. *Initial Reports Deep Sea Drilling Project*, 1:521–593, 1969.

[3] J. Berthelon, A. Brüch, D. Colombo, J. Frey, R. Traby, A. Bouziat, M.-C. Cacas-Stentz, and T. Cornu. Impact of tectonic shortening on fluid overpressure in petroleum system modelling: Insights from the Neuquén basin, argentina. *Marine and Petroleum Geology*, 127:104933, 2021.

[4] M. A. Biot. General theory of three-dimensional consolidation. *Journal of Applied Physics*, 12(2):155–164, 1941.

[5] M. A. Biot and D. G. Willis. The elastic coefficients of the theory of consolidation. *Journal of Applied Mechanics*, 24(4):594–601, 1957.

[6] S. Bloch, J. H. McGowen, and D. W. Brizzolara. Porosity prediction, prior to drilling, in sandstones of the Kekiktuk formation (Mississippian), North slope of Alaska. *American Association of Petroleum Geologists*, 74(9), 1990.

[7] M. Boutéca, J.-P. Sarda, and J. Laurent. Rock mechanics contribution to the determination of fluid flow properties. In *Second European Core Analysis Symposium (Eurocas II)*. London, 1991.

[8] A. Bouziat, N. Guy, J. Frey, D. Colombo, P. Colin, M.-C. Cacas-Stentz, and T. Cornu. An assessment of stress states in passive margin sediments: Iterative hydro-mechanical simulations on basin models and implications for rock failure predictions. *Geosciences*, 9(11):469, 2019.

[9] A. Brüch, D. Colombo, J. Frey, J. Berthelon, M.-C. Cacas-Stentz, and T. Cornu. Poro-elastoplastic constitutive law for coupling 3d geomechanics to classical petroleum system modeling. 54th U.S. Rock Mechanics/Geomechanics Symposium, 2020.

[10] A. Brüch, S. Maghous, F. L. B. Ribeiro, and L. Dormieux. A thermo-poro-mechanical constitutive and numerical model for deformation in sedimentary basins. *Journal of Petroleum Science and Engineering*, 160:313–326, 2018.

[11] P. C. Carman. Fluid flow through granular beds. *Chemical Engineering Research and Design*, 75:S32–S48, 1937.

[12] P. C. Carman. *Flow of Gases through Porous Media*. New York: Academic Press, 1956.

[13] T. Dasgupta and S. Mukherjee. *Compaction of Sediments and Different Compaction Models*, page 1–8. Advances in oil and gas exploration & production. Springer International Publishing, 2020.

[14] F. L. DiMaggio and I. S. Sandler. The effect of strain rate on the constitutive equation of rocks. *Defense Nuclear Agency*, 2801T, 1971.

[15] B. Doligez. Migration of hydrocarbons in sedimentary basins. 2nd IFP Exploration Research Conference, Carcans, France. Institut français du pétrole, 1987.

[16] L. Dormieux and S. Maghous. Poroelasticity and poroplasticity at large strains. *Oil & Gas Science and Technology*, 54(6):773–784, 1999.

[17] P. M. Doyen. Permeability, conductivity, and pore geometry of sandstone. *Journal of Geophysical Research*, 93(B7):7729, 1988.

[18] H. V. Dunnington. Aspects of diagenesis and shape change in stylolitic limestone reservoirs. 7th World Petroleum Congress (WPC), 1967.

[19] EDF R&D. Code Aster. `http://www.code-aster.org`, 2017.

[20] I. Faille, M. Thibaut, M. C. Cacas, P. Havé, F. Willien, S. Wolf, L. Agelas, and S. Pegaz-Fiornet. Modeling fluid flow in faulted basins. *Oil & Gas Science and Technology*, 69(4):529–553, 2014.

[21] A. C. Fowler and X.-S. Yang. Fast and slow compaction in sedimentary basins. *SIAM journal on applied mathematics*, 59(1):365–385, 1998.

[22] H. Fuchtbauer. Influence of different types of diagenesis on sandstone porosity. 7th World Petroleum Congress (WPC), 1967.

[23] M. R. Giles, S. L. Indrelid, and D. M. D. James. Compaction—the great unknown in basin modelling. *Geological Society, London, Special Publications*, 141(1):15–43, 1998.

[24] M. Gutierrez and M. Wangen. Modeling of compaction and overpressuring in sedimentary basins. *Marine and Petroleum Geology*, 22(3):351–363, 2005.

[25] N. Guy, D. Colombo, J. Frey, T. Cornu, and M. C. Cacas-Stentz. Coupled modeling of sedimentary basin and geomechanics: A modified Drucker–Prager cap model to describe rock compaction in tectonic context. *Rock Mechanics and Rock Engineering*, 52(10):3627–3643, 2019.

[26] N. Guy, G. Enchéry, and G. Renard. Numerical modeling of thermal EOR: Comprehensive coupling of an AMR-based model of thermal fluid flow and geomechanics. *Oil & Gas Science and Technology*, 67(6):1019–1027, 2012.

[27] J. Kozeny. Über kapillare Leitung des Wassers im Boden. *Sitzungsberichte der Akademie der Wissenschaften in Wien*, 136(2a):271–306, 1927.

[28] X. Luo, G. Vasseur, A. Pouya, V. Lamoureux-Var, and A. Poliakov. Elasto-plastic deformation of porous media applied to the modelling of compaction at basin scale. *Marine and Petroleum Geology*, 15(2):145–162, 1998.

[29] V. Lyakhovsky, E. Shalev, I. Panteleev, and V. Mubassarova. Directional compaction. *Earth and Space Science Open Archive*, 2020.

[30] S. Maghous, A. Brüch, D. Bernaud, L. Dormieux, and A. L. Braun. Two-dimensional finite element analysis of gravitational and lateral-driven deformation in sedimentary basins. *International Journal for Numerical and Analytical Methods in Geomechanics*, 38(7):725–746, 2014.

[31] H. Marín-Moreno, T. A. Minshull, and R. A. Edwards. A disequilibrium compaction model constrained by seismic data and application to overpressure generation in the Eastern Black Sea basin. *Basin Research*, 25(3):331–347, 2013.

[32] J. Obradors-Prats, M. Rouainia, A. C. Aplin, and A. J. L. Crook. Assessing the implications of tectonic compaction on pore pressure using a coupled geomechanical approach. *Marine and Petroleum Geology*, 79:31–43, 2017.

[33] K. S. Okiongbo. Effective stress-porosity relationship above and within the oil window in the north sea basin. *Research Journal of Applied Sciences, Engineering and Technology*, 2011.

[34] V. Schmidt and D. A. McDonald. The role of secondary porosity in the course of sandstone diagenesis. In *Aspects of Diagenesis*. SEPM Society for Sedimentary Geology, 1979.

[35] F. Schneider. Modèle de compaction élasto-plastique en simulation de bassins. *Revue de l'Institut Français du Pétrole*, 48(1):3–14, 1993.

[36] F. Schneider, J. Burrus, and S. Wolf. Modelling overpressures by effective-stress/porosity relationships in low-permeability rocks: Empirical artifice or physical reality. *Norwegian Petroleum Society Special Publications*, 1993.

[37] F. Schneider and S. Hay. *Compaction Model for Quartzose Sandstones - Application to the Garn Formation, Haltenbanken, Mid-Norwegian Continental Shelf - Part I - Theory*. European Association of Geoscientists & Engineers, 2001.

[38] F. Schneider, J. L. Potdevin, S. Wolf, and I. Faille. Modèle de compaction élastoplastique et viscoplastique pour simulation de bassins sédimentaires. *Revue de l'Institut Français du Pétrole*, 49(2):1–8, 1994.

[39] F. Schneider, J. L. Potdevin, S. Wolf, and I. Faille. Mechanical and chemical compaction model for sedimentary basin simulators. *Tectonophysics*, 263(1–4):307–317, 1996.

[40] F. Schneider, S. Wolf, I. Faille, and D. Pot. A 3d basin model for hydrocarbon potential evaluation: application to Congo offshore. *Oil & Gas Science and Technology*, 55(1):3–13, 2000.

[41] K. Terzaghi. Die Berechnung der Durchlassigkeitsziffer des Tones aus dem Verlauf der Hidrodynamichen Spannungserscheinungen. *Akademie der Wissenschaften in Wien*, 132:125–138, 1923.

[42] P. Ungerer, J. Burrus, B. Doligez, P. Y. Chenet, and F. Bessis. Basin evaluation by integrated two-dimensional modeling of heat transfer, fluid flow, hydrocarbon generation, and migration. *American Association of Petroleum Geologists*, 74(3), 1990.

[43] Y. Yang and A. C. Aplin. A permeability-porosity relationship for mudstones. *Marine and Petroleum Geology*, 27(8):1692–1697, 2010.